Journal of Materials Chemistry C

Accepted Manuscript

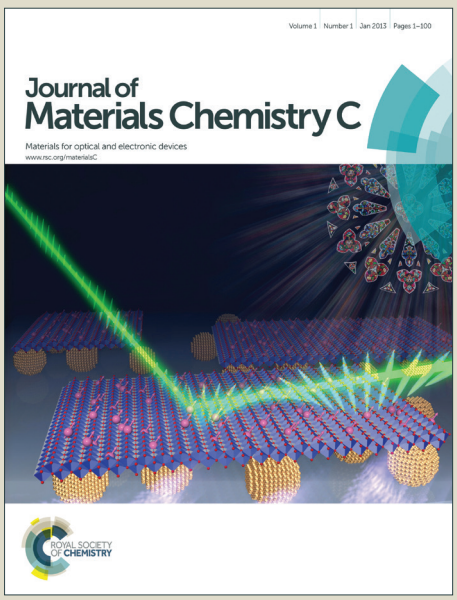

ROYAL SOCIETY OF CHEMISTRY

www.rsc.org/materialsC

Journal Name

RSCPublishing

COMMUNICATION

The Curious Case of CdTe/CdS: Photoabsorption versus Photoemission

Cite this: DOI: 10.1039/xoxxoooooox

Avijit Saha,[a] Soma Chattopadhyay,[b] Tomohiro Shibata,[b] and Ranjani Viswanatha*[,a,c]

Received ooth January 2012,
Accepted ooth January 2012

DOI: 10.1039/xoxxoooooox

www.rsc.org/

The potential of nanomaterials arises from the fine tuning of material properties by changing composition, size and shape. Here we show that by varying the local Cd and Te/S environment using CdTe/CdS as the host, a highly promising photovoltaic material can easily be converted to an efficient photo-emitting material. Thus we demonstrate for the first time that internal structure can be used to tune the properties of the nanomaterial leading to competing and contrasting applications.

The Nanocrystal quantum dots (NQDs), with an emphasis to develop novel colloidal nanomaterials for energy harvesting[1, 2] and conversion applications[3], have been the subject of current research. Size, shape and composition[4] dependence of the chemical and physical properties of NQDs[5] have shown potential as promising materials for a diverse set of applications including as active materials in photovoltaics[6, 7] and as size tunable phosphors[8, 9] in lighting and displays.[10-13] This has propelled efforts toward controlled synthesis and in-depth characterization with programmable composition and geometric features. However, until recently, the effect of internal crystal structure of NQDs on the properties of the material is not systematically studied. In recent times, with the introduction of ultra high resolution TEM[14] as well as X-ray photoemission,[15] the dramatic effect of lattice defects on the photo-physical properties like quantum yield, blinking etc have come to light. Here in this report, we show that lattice defect engineering provides a playground to regulate the electron hole overlap[16] particularly in type II semiconductor interfaces[17] leading to efficient photo-absorber as well as a photo-emitter obtained from the same material. This is interesting given that photovoltaics[23] ultimately aim to absorb light, and convert the photogenerated excitons into spatially separate electrons and holes. On the other hand, the quality of the photoemitter[11, 12, 18] is regulated by the efficiency of the recombination of the electron-hole pair leading to the emission of the absorbed energy. This naturally implies that photo-absorptive materials are in general not efficient as active materials for a photo-emitting device and vice versa.

CdTe, with high optical absorption coefficient and optimum bandgap for solar photovoltaics,[19] and a perfect match of electron affinity of CdS[20] in addition to the type II bandgap at the heterojunction of the CdTe and CdS have led to the widespread use of CdTe/CdS as active materials for photovoltaic devices[21] with cell efficiencies as high as 16%.[22] However, it is so far, not extensively used as a photo-emissive material for the well known reason of low quantum yield. Nevertheless, in this report, we observe that CdTe core NQDs synthesis dictates the photophysical properties giving rise to both photo-emitting high quantum yield (QY) materials as well as low QY, long lifetime materials suitable for photovoltaic applications. We use X-ray diffraction (XRD) and extended x-ray absorption fine structure (EXAFS) to study the long range and short range structure respectively explaining the photoluminescence properties of QY and excited state lifetime obtained from time resolved photoluminescence (TrPL).

Experimental

Materials. Cadmium oxide (CdO), oleic Acid (OA, 90%), 1-octadecene (ODE, 90%), trioctylphosphine oxide (TOPO, 90%), oleylamine (OlAm, 70%), trioctylphosphine (TOP, 90%) Te shots and sulphur powder (99.5%) were purchased from Sigma Aldrich. Cadmium acetate dihydrate ($Cd(ac)_2$) was purchased from sd fine-chem limited. All these chemicals were used without further purification.

The synthesis of CdTe cores (CdTe-A and CdTe-C) were carried out using two different synthesis methods described below. Further overcoating of these core NQDs with CdS was carried out using successive ionic layer adsorption and reaction

(SILAR) technique with alternate addition of Cd and S precursors followed by annealing at high temperature.

Synthesis of CdTe core QDs for CdTe-C: CdTe-C NQDs were synthesized after minor modification of literature method.[23] Briefly, 0.4 M TOP/Te solution was prepared by dissolving Te shots in TOP inside a glove box. In a typical synthesis method, 0.2 mmol (25.6 mg) of CdO, 0.2 ml of oleic acid, 8 ml of ODE were taken in a three necked round bottom flask. The temperature was maintained at 80°C for degassing under vigorous stirring. After degassing, temperature of the reaction mixture was raised to 310°C under constant Ar flow. After 30-40 min, as soon as a white coloured precipitate appeared, the temperature was brought down to 290°C and a solution containing 0.13 ml of TOP/Te diluted with 1ml of TOP and 1.12 ml of ODE was quickly injected into the hot mixture. After a few seconds, the temperature was quickly quenched down to room temperature using ice bath. Samples were washed twice by centrifugation using hexane and methanol mixture.

Synthesis of CdTe core QDs for CdTe-A: In a typical synthesis, 20 mg (0.075 mmol) Cadmium acetate dihydrate, 0.3 ml of oleic acid, 0.4 gm of TOPO and 5ml of ODE were taken in a three necked flask and degassed at 80°C under constant stirring. 3 ml TOP was added into this reaction mixture during this procedure. Te precursor was prepared using 0.1 ml of 0.4 M TOP/Te solution mixed with 0.9 ml of TOP and 1ml of ODE. After degassing, the temperature was raised to 320°C under steady Ar flow. At 320°C the TOP/Te was injected to the hot reaction mixture and the temperature was quenched down to room temperature using ice bath after a few seconds. Similar to the previous CdTe core, samples were washed and preserved for further use.

Overcoating of CdS shell on CdTe (CdTe-C/shell and CdTe-A/shell): SILAR technique[24] was followed to synthesize these core/shell NQDs. Firstly, 0.2 M cadmium oleate ($Cd(OA)_2$) and 0.2 M sulphur precursor were prepared using well known literature methods. The stoichiometric amount of Cd and S precursor required for each individual layer was calculated and added in a stepwise addition. In a typical experiment, CdTe cores (1×10^{-7} mol), 3 ml of OlAm and 4 ml of ODE were taken into a round bottom flask and degassed under vacuum with the temperature gradually increased to 70°C. After degassing the reaction flask was backfilled with Ar and the temperature was raised to 170°C and required amount of $Cd(OA)_2$ for the first shell was injected into the reaction mixture. After 10/15 min, the temperature was further raised to 220°C and same amount of S precursor was injected into the reaction. After 5/10 min, cycles of Cd followed by S precursors were injected and annealed at this temperature for all subsequent shell formation. The annealing conditions were very similar for both CdTe-A and CdTe-C NQDs except small changes in annealing time that was done to further exemplify the results. In both the cases, aliquots were taken out after completion of each monolayer addition. All the samples were washed by centrifugation using hexane methanol mixture and redissolved in hexane.

Chracterization

TEM was performed on a Technai F30 UHR version electron microscope, using a field emission gun (FEG) operating at an accelerating voltage of 200 kV. Absorption spectra of samples were recorded using Agilent 8453 UV-visible spectrometer. Steady state PL spectra were obtained using a 450 W xenon lamp as the source on the FLSP920 spectrometer, Edinburgh instrument, while the lifetime measurements were carried out using the EPL-405 ps pulsed diode laser. QY of the nanocrystals were determined using 'integrating sphere', an absolute QY measurement system, Edinburgh instrument. X-ray diffraction patterns for the NQDs were recorded on Bruker D8 Advance diffractometer using Cu-Kα radiation. The Cd K-edge (26711 eV) and Te K-edge (31814 eV) EXAFS measurements were carried out at the MRCAT 10-ID beam line at the Advanced Photon Source, Argonne National Laboratory[25] The data was collected in fluorescence Stern-Heald geometry with samples loaded in cylindrical cuvettes. Cd foil and Te powder tapes were measured in transmission geometry with help of the reference ion chamber for every scan taken at Cd edge and Te edge respectively. The spot size of the incident x-ray beam on the sample was 500 micron by 500 micron. Platinum mirror was used for harmonic rejection. Incident ion chamber had full nitrogen gas; transmission and reference ion chambers were filled with 80% Argon mixed with 20% nitrogen. Fluorescence ion chamber had Krypton gas. Data collected was processed using Athena software[26] by extracting the EXAFS oscillations $\chi(k)$ as a function of photoelectron wave number k. The theoretical paths were generated using FEFF6[27] and the models were done in the conventional way using the fitting program called Artemis.[28] Fitting parameters were obtained by modeling the EXAFS data of each sample in R-space until a satisfactory fit describing the system was obtained. Data sets were simultaneously fitted in R-space with k-weights of 1, 2 and 3.

Results and Discussion

Typical transmission electron microscope (TEM) images of the cores and the CdS overcoated materials along with their size distribution analysis are shown in Fig. 1. From the figure it is evident that both the sizes of the two cores (4.1 nm and 4.5 nm) and the overcoated (6.4 nm and 6.8 nm) materials are very similar. In order to obtain the actual concentration of Te to S ratio, we performed an inductively coupled plasma atomic emission spectroscopy (ICP-AES) measurements and found that the Te/S ratio in the two materials are very similar.

However, in spite of similar particle size, the absorption and photoluminescence characteristics of the two materials were unexpectedly found to be dramatically different. Figure 2(a) shows the evolution of absorption (dotted line) and emission spectra (solid line) of the NQDs during the growth of the CdS shell on CdTe-C cores emitting at 2.09 eV with a sharp absorption peak at 2.15 eV. As expected, CdS shell leads to broadening eventually smearing out of the absorption feature completely along with a shift to lower energies. The smearing

is also accompanied by a significant increase in the Stoke's shift between the absorption feature and the emission energy. This observation of lower energy transitions due to weak spatially indirect transitions is consistent with the formation of a type-II structure as expected from the alignment of the energy states. Further signatures of type II semiconductors is observed in the TrPL data shown in Fig. 2(b) as well as the evolution of QY as a function of shell formation as shown in Fig. 2(c). The electron-hole recombination lifetime increases with increasing shell thickness as shown in Fig. 2(b) and the average lifetime (red) plotted in Fig. 2(c). Though the QY initially increases due to the surface protection of CdTe, it eventually decreases due to the "spatially indirect" nature of the electron-hole pair leading to lower efficiency of radiative recombination. From this it is evident that this CdTe/CdS indeed forms a type-II interface.

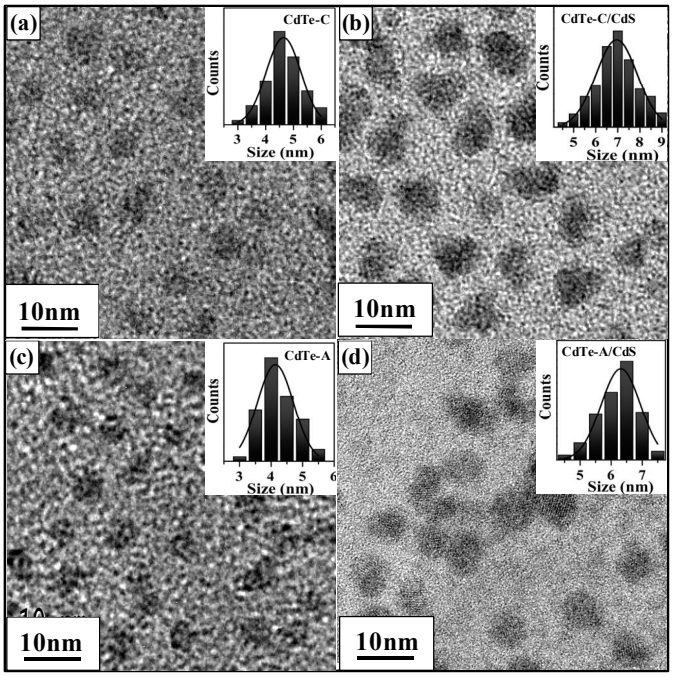

Fig 1. TEM images of (a) 4.5 nm CdTe-C and (b) 6.8 nm CdTe-C/CdS (c) 4.1 nm CdTe-A (d) 6.4 nm CdTe-A/CdS NQDs and their size distributions are shown in the corresponding insets showing the formation of spherical NQDs of specified sizes.

In contrast, the optical characterization obtained from CdTe-A samples show unexpectedly different behaviour as shown in Fig. 3. Figure 3(a) shows the evolution of absorption (dotted line) and emission spectra (solid line) of the NQDs during the growth of the CdS shell on CdTe-A cores. However it is obvious that the absorption edge is much sharper in CdTe-A/CdS samples compared to the CdTe-C/CdS samples, as shown by a typical example in the supporting information Fig S1. Nevertheless, it is interesting to note that the Stokes shift in the case of CdTe-A/CdS is not as high as expected for type II systems and is contributed from both, a minute red shift of the absorption edge and a tiny blue shift of emission peak as observed in Fig. 3(a). In addition the difference in the emission energy of 1.8 eV in 6.4 nm CdTe-A/CdS (Fig. 3(a)) compared to 1.4 eV in 6.8 nm CdTe-C/CdS (Fig. 2(a)) cannot be explained either by experimental error or as a consequence of small changes in the size of the nanocrystals (~0.4 nm). In fact, the small Stokes shift is suggestive of a direct transition instead of the expected indirect transition. More interestingly, the lifetime and quantum yield of these materials show drastic changes as seen in Figs. 2b, 2c, 3b and 3c. From the Fig. 3b and 3c, it is apparent that the lifetime of the excitonic recombination of CdTe-A/CdS does not increase with increasing shell thickness and retains a high QY of ~ 80% in the thickest shell sample consistent with the absorption and the emission data. These changes in the absorption and emission energy as well as lifetime and QY measurements provide clear signatures of spatially direct recombination of the charge carriers within the heterostructure in an established type-II band structure alignment.[29]

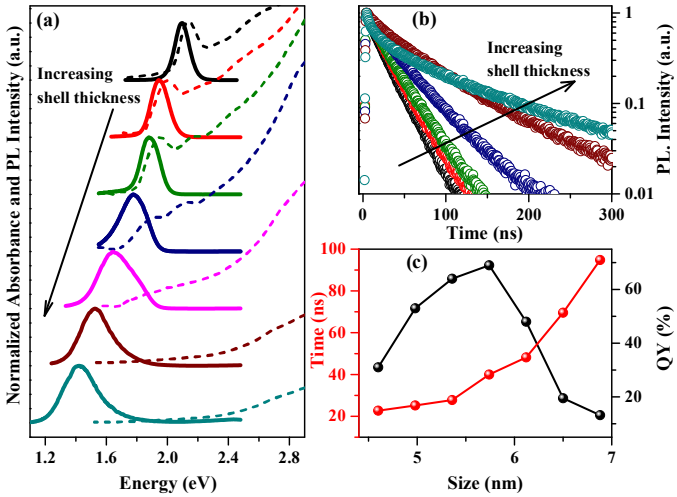

Fig. 2. (a) Absorption (dotted line) and PL (solid lines) of CdTe-C core and CdTe-C/CdS nanocrystals with increasing CdS shell. (b) Lifetime decay plots for core CdTe-C and CdTe-C/CdS nanocrystals. (c) The variation of QY (black) and average lifetime (red) as a function of size starting from core CdTe-C to CdTe-C/CdS nanocrystals. (Dots show experimental points and lines show guide to the eye).

These qualitative differences in the nature of the optical properties based on quantitative changes in the synthesis parameters is remarkable and could have far-reaching consequences in applications if the origin of this anomalous effect can be understood from a fundamental perspective. The recent study of the internal structures of NQDs,[14] so far only lightly explored, have shown the potential of such a study to understand these unusual photo-physical properties. In the present case, our study of the properties of the core with an average lifetime of 22.6 ns and a QY of 30.5% in CdTe-C and 18.5 ns and 18% respectively for CdTe-A suggests that CdTe-C has a lower percentage of non-radiative decay pathways and higher QY compared to CdTe-A suggesting the presence of more surface defects in CdTe-A cores. In fact, detailed analysis of the synthesis procedure suggests that in the case of CdTe-C, the cores were synthesized by heating at 310^{0}C for 30-45

minutes until a cloudy white precipitate of Cd^0 nanoparticles forms which reacts with TOP/Te and forms high quality QDs. This formation of Cd^0 nanoparticles in a thermodynamically slow process ensures that the surface is properly formed and well passivated upon injection of Te complex. However, in case of CdTe-A cores, Te complex is injected as soon as the temperature of the Cd precursor reaches 320°C. In this case TOP-Te reacts with Cd-oleate complex rather than Cd^0 nanoparticles which gives rise to comparatively more surface defects than CdTe-C. However, this is only one of the factors and the formation of surface defects in NQDs depends on various factors including temperature, anealing time at high temperature, ligands[30] used and its concentration. Surface defective cores are known to be viable for efficient alloy formation[14] at the interfaces. Analogous judgment in the current scenario would lead to the formation of alloyed interface[31] in the case of CdTe-A/CdS. The results of such a variation in structure can be elucidated as shown in the schematic in Fig. 4(a) and 4(b). Formation of a sharp interface combined with a type-II alignment[32] leads to the lower overlap of e-h wavefunction resulting a "spatially indirect" recombination. However, formation of an alloy at the interface leads to a more "spatially direct" recombination due to the greater e-h wavefunction overlap. This conjecture is verified using long-range and short range crystal structure analysis as shown in Fig. 4(c) to Fig. 4(e) using X-ray diffraction and EXAFS spectroscopy.

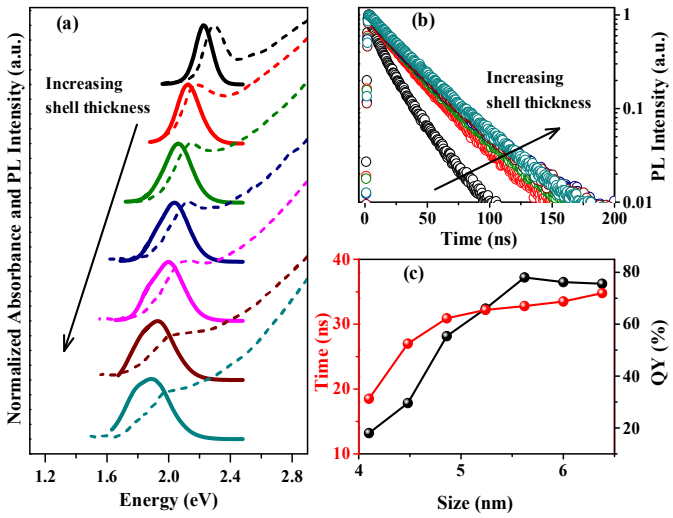

Fig. 3. (a) Absorption (dotted lines) and PL (solid lines) of CdTe-A core and CdTe-A/CdS nanocrystals with increasing CdS. (b) Lifetime decay plots for core CdTe-A and CdTe-A/CdS nanocrystals. (c) The variation of QY (black) and average lifetime (red) as a function of size starting from core CdTe-A to CdTe-A/CdS nanocrystals. (Dots show experimental points and lines show guide to the eye.)

The XRD patterns shown in Fig. 4(c) illustrate that while the crystal structures of CdTe-A and CdTe-C matches with that of cubic CdTe (bulk), the peaks of CdTe-A/CdS is only slightly shifted compared to CdTe-A with no characteristic Cd-S peaks. Contrastingly, clear signatures of both CdS and CdTe lattices are observed in CdTe-C/CdS. These observations are in agreement with an alloyed interface in CdTe-A/CdS as discussed earlier in the text. This is further confirmed by the local structure analysis around the Cd and Te atoms using EXAFS spectroscopy. The Fourier transform of the Cd and Te K-edge EXAFS with their corresponding fitting is shown in Fig. 4(d) and 4(e) respectively while the Cd and Te K-edges with evidences of surface oxidation are shown in the supporting information, Fig. S2 and S3 respectively. The fitting parameters are shown in Table S1 and S2 in the supporting information. The presence of Cd-Te bond (~2.5 Å, green line) and the Cd-S (1.9 Å, magenta line) in CdTe-C/CdS compared to a single major peak in CdTe-A/CdS with a slightly larger bond length is in agreement with the XRD data. This suggests that CdTe-A/CdS is most likely an alloy of CdTe and CdS with its bond length close to CdS structure. This is further validated by the Te K-edge in these samples as shown in Fig.4(e) and Fig. S3. The local environment around the Te in CdTe-C/CdS can be simply explained with Cd-Te bond and Te-Te bond, while Te oxidation is evident in CdTe-A/CdS suggesting that Te is exposed to the atmosphere. Thus the various signatures in EXAFS are consistent with the formation of an alloy structure in CdTe-A/CdS.

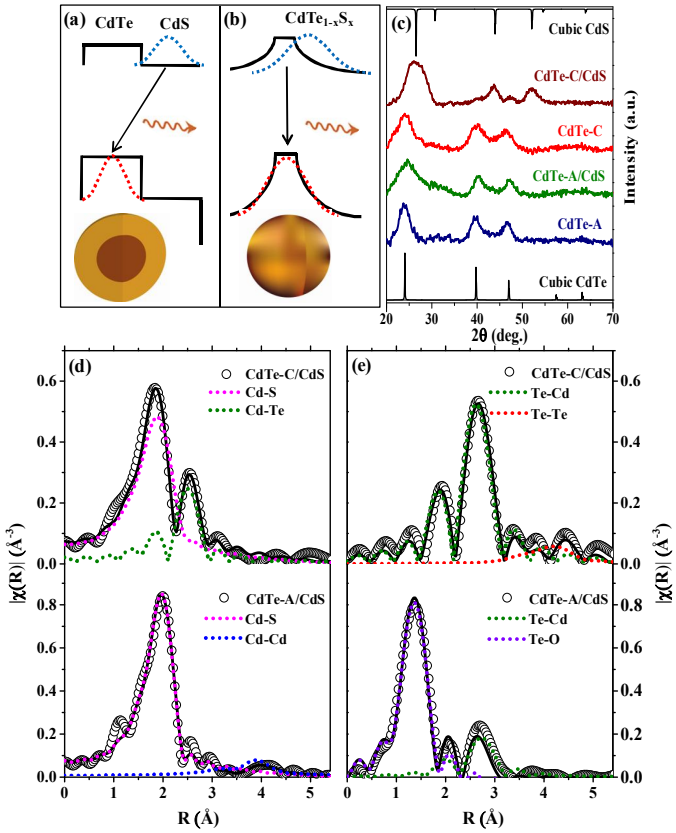

Fig. 4. Schematics of CdTe/CdS (a) core/shell structure with spatially non-overlapping and (b) alloy interface with spatially overlapping electron (blue) and hole (red) wavefunction and their relative bandgap alignment[32] for the largest size of CdTe/CdS. (c) XRD patterns of the different CdTe cores, CdTe-A/CdS and CdTe-C/CdS nanocrystals along with the bulk cubic CdTe and CdS. FT of experimental (d) Cd-edge and (e) Te-edge EXAFS spectra (circles) and their fits (solid lines)

for CdTe-C/CdS and CdTe-A/CdS. Dotted lines show different fitting paths.

Conclusions

Thus these data conclusively proves that surface defects in NQDs can be used to radically alter the properties of the NQDs leading to contrasting applications like photoemission and photoabsorption. Consequently, the synthesis parameters can be tuned to obtain properties necessary for the applications. These origins can be successfully traced to the lattice defects as obtained from spectroscopic techniques like EXAFS, x-ray photoemission and diffraction methods. In conclusion, we have shown in this work that lattice defects can indeed play a very important role in determining the properties of the nanomaterials and is as strong a handle as that of size or shape of NQDs. We then demonstrated this principle for specific case of CdTe/CdS semiconductor heterostructures.

Corresponding Author

*Email: rv@jncasr.ac.in.

Acknowledgement

AS and RV thank JNCASR, Sheikh Saqr Laboratory and Department of Science and Technology, Government of India for financial support. AS thanks CSIR for a research fellowship. We thank Dr. Vladislav Zyryanov for designing the sample cells for EXAFS. MRCAT operations are supported by the Department of Energy and the MRCAT member institutions. Use of the Advanced Photon Source, an Office of Science User Facilities operated for the U. S. Department of Energy (DOE) Office of Science by Argonne National Laboratory, was supported by the U.S. DOE under Contract No. DE-AC02-06CH11357.

Notes and references

[a] New Chemistry Unit, Jawaharlal Nehru Centre for Advanced Scientific Research, Jakkur, Bangalore - 560064, India
[b]CSRRI-IIT, MRCAT, Sector 10, Bldg 433B, Argonne, National Laboratory, Argonne, IL 60439 USA and Physics Department, Illinois Institute of Technology, Chicago, IL 60616 USA.
[c]International Centre for Materials Science, Jawaharlal Nehru Centre for Advanced Scientific Research, Jakkur, Bangalore - 560064, India.

Electronic Supplementary Information (ESI) available: [Absorption spectra, XANES, list of fit parameters]. See DOI: 10.1039/c000000x/

1. Z. L. Wang and W. Wu, *Angew. Chem.*, 2012, **51**, 11700-11721.
2. L. Li, S. Chen, X. Wang, Y. Bando and D. Golberg, *Energy Environ. Sci.*, 2012, **5**, 6040-6046.
3. Q. Zhang, E. Uchaker, S. L. Candelaria and G. Cao, *Chem. Soc. Rev.*, 2013, **42**, 3127-3171.
4. T. P. A. Ruberu, H. R. Albright, B. Callis, B. Ward, J. Cisneros, H.-J. Fan and J. Vela, *ACS Nano*, 2012, **6**, 5348-5359.
5. Y. Guo, K. Marchuk, S. Sampat, R. Abraham, N. Fang, A. V. Malko and J. Vela, *J. Phys. Chem. C*, 2012, **116**, 2791-2800.
6. P. V. Kamat, *J. Phys. Chem. C*, 2008, **112**, 18737-18753.
7. J. Bang, J. Park, J. H. Lee, N. Won, J. Nam, J. Lim, B. Y. Chang, H. J. Lee, B. Chon, J. Shin, J. B. Park, J. H. Choi, K. Cho, S. M. Park, T. Joo and S. Kim, *Chem. Mater.*, 2010, **22**, 233-240.
8. C. C. Lin and R.-S. Liu, *J. Phys. Chem. Lett.*, 2011, **2**, 1268-1277.
9. H. A. Höppe Dr., *Angew. Chem.*, 2009, **48**, 3572-3582.
10. D. D. Sarma, A. Nag, P. K. Santra, A. Kumar, S. Sapra and P. Mahadevan, *J. Phys. Chem. Lett.*, 2010, **1**, 2149-2153.
11. W.-S. Song and H. Yang, *Chem. Mater.*, 2012, **24**, 1961-1967.
12. S. Kim, S. H. Im and S.-W. Kim, *Nanoscale*, 2013, **5**, 5205-5214.
13. W. Ji, P. Jing and J. Zhao, *J. Mater. Chem. C*, 2013, **1**, 470-476.
14. A. Saha, K. V. Chellappan, K. S. Narayan, J. Ghatak, R. Datta and R. Viswanatha, *J. Phys. Chem. Lett.*, 2013, **4**, 3544-3549.
15. P. K. Santra, R. Viswanatha, S. M. Daniels, N. L. Pickett, J. M. Smith, P. O'Brien and D. D. Sarma, *J. Am. Chem. Soc.*, 2009, **131**, 470-477.
16. A. Pandey and P. Guyot-Sionnest, *J. Chem. Phys.*, 2007, **127**, 111104-111104.
17. X. Li, H. Shen, S. Li, J. Z. Niu, H. Wang and L. S. Li, *J. Mater. Chem.*, 2010, **20**, 923-928.
18. W. Ji, P. Jing, J. Zhao, X. Liu, A. Wang and H. Li, *Nanoscale*, 2013, **5**, 3474-3480.
19. R. Debnath, O. Bakr and E. H. Sargent, *Energy Environ. Sci.*, 2012, **4**, 4870-4881.
20. M. Shalom, S. Ruhle, I. Hod, S. Yahav and A. Zaban, *J. Am. Chem. Soc.*, 2009, **131**, 9876-9877.
21. X.-Y. Yu, B.-X. Lei, D.-B. Kuang and C.-Y. Su, *Chem.Sci.*, 2011, **2**, 1396-1400.
22. S. G. Kumar and K. S. R. K. Rao, *Energy Environ. Sci.*, 2014, **7**, 45-102.
23. V. Kloper, R. Osovsky, J. Kolny-Olesiak, A. Sashchiuk and E. Lifshitz, *J. Phys. Chem. Lett.*, 2007, **111**, 10336-10341.
24. J. J. Li, Y. A. Wang, W. Guo, J. C. Keay, T. D. Mishima, M. B. Johnson and X. Peng, *J. Am. Chem. Soc.*, 2003, **125**, 12567-12575.
25. C. U. Segre, N. E. Leyarovska, L. D. Chapman, W. M. Lavender, P. W. Plag, A. S. King, A. J. Kropf, B. A. Bunker, K. M. Kemner, P. Dutta, R. S. Duran and J. Kaduk, *AIP Conf. Proc.*, 2000, **521**, 419-422.
26. M. Newville, *J. Synchr. Radn.*, 2001, **8**, 322-324.
27. J. J. Rehr and R. C. Albers, *Rev. Mod. Phys.*, 2000, **72**, 621-654.
28. B. Ravel and M. Newville, *J. Synchr. Radn.*, 2005, **12**, 537-541.
29. L. z. Borg, D. Lee, J. Lim, W. K. Bae, M. Park, S. Lee, C. Lee, K. Char and R. Zentel, *J. Mater. Chem. C*, 2013, **1**, 1722-1726.
30. N. Mishra, J. Lian, S. Chakrabortty, M. Lin and Y. Chan, *Chem. Mater.*, 2012, **24**, 2040-2046.
31. K. Boldt, N. Kirkwood, G. A. Beane and P. Mulvaney, *Chem. Mater.*, 2013, **25**, 4731-4738.
32. G. K. Grandhi, R. Tomar and R. Viswanatha, *ACS Nano*, 2012, **6**, 9751-9763.

Table of content: Internal structure joins the family of property tunability of quantum dots.